Fuel 317 (2022) 123570

Contents lists available at ScienceDirect

Fuel

journal homepage: www.elsevier.com/locate/fuel

Full Length Article

Potassium release during pulverized biomass combustion in a tubular burner investigated by TDLAS

Sun Cen [a,b], Wei Xiaolin [a,b,*], Li Teng [a,b], Zhou Li [c], Teng Qinzheng [a,b], Li Sen [a,b]

[a] State Key Laboratory of High-Temperature Gas Kinetics, Institute of Mechanics, Chinese Academy of Sciences, Beijing 100190, China
[b] School of Engineering Science, University of Chinese Academy of Sciences, Beijing 100049, China
[c] School of Energy and Power Engineering, Xi'an Jiaotong University, Xi'an 710049, China

ARTICLE INFO

Keywords:
Biomass
Alkali metal
Tunable diode laser absorption spectroscopy
Tubular burner

ABSTRACT

The ignition and effect of different treatments of pulverized biomass on potassium release were monitored online using visible light detection and calibration-free TDLAS techniques in a tubular burner, with the following main conclusions. High-speed cyclonic flow enhanced the transport effect around the particles, allowing for the rapid separation and diffusion of volatile fractions from biomass particles, as well as the rapid but transient release of potassium. There were no visible envelope flames or trailing flames around the burning particles. High-speed photography also confirmed the homo-heterogeneous ignition. The release of water-soluble potassium was significantly postponed under an O_2/CO_2 atmosphere compared with the air atmosphere, shifting from a quick and instantaneous model to a continuous and slow-release one. In comparison, the O_2/CO_2 atmosphere had little suppression effect on the exchangeable and organic potassium release process. In both air and O_2/CO_2 combustion, the water-soluble potassium release was the fastest, followed by organic potassium and exchangeable state potassium. The release ratio of atomic potassium, the proportion of released atomic potassium in initial total potassium in particles, from water-washed and NH_3Ac-washed rice husk is higher than that from rice husk combustion, under O_2/CO_2 and O_2/N_2 combustion conditions. The release process of potassium enriched in char takes a long time but has a low release rate. The inhibitory effect of the O_2/CO_2 atmosphere on the potassium release during rice husk char combustion was relatively weak compared with rice husk combustion.

1. Introduction

The utilization of biomass fuels has received increased importance in China's 2050 carbon reduction and renewable energy goals; however, the emission of alkali metals during biomass combustion can induce the scaling and corrosion of boiler heating surfaces. Understanding the release characteristics of alkali metals during the combustion of high-alkali solid fuels is essential for their practical utilization.

Many fundamental studies have investigated and measured the ignition and combustion processes of biomass using optical diagnostic techniques. There have been few studies on the igniting mechanism of pulverized biomass. Simóes et al. [1] performed a detailed study of pulverized biomass's ignition behavior, including the ignition of wheat straw in a laminar flame using high-speed photography. They observed that biomass particles ignited in the gas phase. Utilizing a hyperspectral imager, Si et al. [2] recorded the combustion process of pulverized coal on a McKenna flat flame burner and discovered that pulverized coal exhibited homogeneous ignition characteristics. Qi et al. [3] employed an ICCD camera with a 430 nm band-pass filter to capture CH* chemiluminescence images on a Henken burner and discovered that biomass and lignite particles ignited homogeneously in both air and oxy-fuel environments. Temporal and spectral resolution and CH* chemiluminescence at various phases of biomass conversion were recorded by Fatehi [4], and numerical work was performed to investigate the ignition behavior for pulverized biomass. Overall flame structure and heterogeneous reaction on the surface of char under turbulent flow can be well reproduced by the numerical simulations combined with turbulence-chemistry interaction models [5–8]; however, the effect of turbulence and O_2/CO_2 combustion on pulverized biomass's ignition and alkali metal release behavior still needs further experimental observations critically.

Due to biomass's high potassium content, there is a need to obtain

* Corresponding author.
E-mail addresses: suncener@163.com (S. Cen), xlwei@imech.ac.cn (W. Xiaolin), liteng@imech.ac.cn (L. Teng), zhou15930717928@stu.xjtu.edu.cn (Z. Li), tengqinzheng@imech.ac.cn (T. Qinzheng), lisen@imech.ac.cn (L. Sen).

https://doi.org/10.1016/j.fuel.2022.123570
Received 27 October 2021; Received in revised form 5 February 2022; Accepted 8 February 2022
Available online 15 February 2022
0016-2361/© 2022 Elsevier Ltd. All rights reserved.

quantitative information about the release characteristics of alkali species to ensure the optimal control of coking and slagging during high-alkaline biomass utilization. Using planar laser-induced fluorescence (PLIF) [9–12], the release processes of potassium/sodium from coal/biomass/char pellets hung over a planar flame burner were detected online. Along with the PLIF technology, laser-induced breakdown spectroscopy (LIBS) is also commonly used to assess alkali metals' quantitative and temporal release properties in a plume of coal or biomass pellets in a flat flame [13,14]. He et al. [15–17] quantified the release processes of different forms of alkali metalmetals and the alkali metals' adsorption capacity for different sorbent additives (silica, alumina, kaolin, mica, etc.) under O_2/CO_2 combustion atmospheres. Liu et al. [18,19] proposed a multipoint LIBS method for the quantitative measurement of the sodium concentration in the gas phase during the combustion of coal pellets. Ye Yuan et al. [20] developed a low-intensity LIBS technique to distinguish between solid-phase and gas-phase sodium during combustion. They found that the ambient temperature played the dominant role in the transition from solid-phase sodium to gas-phase sodium. By investigating the spontaneous emission spectrum of potassium, He et al. [21] discovered that the proportion of potassium released during the devolatilization and ash stages was higher than that during the char burning stage. Li et al. [22] quantified the potassium released from rice straw pellet during the volatiles and char combustion stages. PLIF, LIBS, and emission spectroscopy have been used in these online potassium monitoring studies, but each of these techniques requires calibration procedures and is subject to interference by stray light, self-absorption, and soot. Tunable diode laser absorption spectroscopy (TDLAS) has an inexpensive, compact sensor and allows for the rapid, selective, and precise quantitative measurement of specific combustion species without the need for calibration in a sooty environment. It has been utilized in full-scale furnaces [23]. However, few studies have used TDLAS technology to monitor alkali metal release processes online [24], and only Umea University has conducted relevant experimental research. Utilizing the TDLAS technique, Schmidt et al. [25] measured the potassium content in the combustion flue gas of wood and straw pellets on a fixed-bed burner. Weng et al. [26] measured the potassium concentration in the combustion plume of individual coal and biomass pellets on a laminar premixed burner.

Most of these investigations have been carried out in laboratory-scale entrained flow reactors, Hencken planar flame burners, or McKenna burners. These laboratory-scale burners have uniform component distributions with low Reynolds numbers and can only offer a laminar flow environment for ignition experiments. Turbulence effects become non-negligible when scaled up to industrial or pilot chambers.

On the other hand, most of the above-mentioned studies focused on biomass/bio-char pellets and relatively few used pulverized biomass, which is typically used in combustion and gasification processes [27,28]. The alkali metal release and combustion processes of biomass pellets may differ from those of micron-sized pulverized biomass utilized in pulverized biomass incinerators. O_2/CO_2 combustion will probably be an important method for reducing future carbon emissions. Therefore, it is essential to quantify the potassium release characteristics from pulverized materials during O_2/N_2 or O_2/CO_2 combustion, especially for particles moving in turbulent environments.

Tubular burner combustion chambers have no swirl blades or blunt bodies, and a tangential jet-induced cyclonic flow stabilizes the distinctive tubular flame. Tubular flames are virtually adiabatic and kinetically stable, and the gas temperature distribution inside the flame is very uniform after combustion, making tubular burners excellent heating equipment [29]. Compared with the flat flame burner or carried flow-flame burner, this ignition technique is more similar to that of a tangentially fired furnace.

Therefore, to perform experiments in a more realistic setting and integrate the behavior of potassium in biomass pyrolysis and biomass char combustion, we utilized a tubular burner to conduct the online detection of pulverized biomass and its char O_2/N_2 or O_2/CO_2 combustion. Combining high-speed imaging with TDLAS technology, we investigated the ignition and potassium release characteristics of pulverized biomass and its char under high turbulent conditions under both O_2/N_2 and O_2/CO_2 atmospheres. This work provides reliable data for the clean combustion of biomass and alkali metal release models.

2. Experimental setup

2.1. Fuel analysis

Rice husk samples from Huainan had a particle size range of 90–120 um, which is comparable in size to those used in pulverized biomass incinerators. Table 1 illustrates the proximity and ultimate analyses performed following China National Standard (GB/T28731-2012).

Note: ad = air-dry basis. The AD (air-dried) basis neglects the presence of moisture other than inherent moisture; M, moisture content; A, ash content; V, volatile matter content; C, carbon content; H, hydrogen content; S, sulfur content; N, nitrogen content.

Rice husk char was prepared in a fixed-bed reactor. Before the experiment, the reactor was preheated to 900 °C and purged with N_2 for 10 min. Rice husk was quickly added and removed after pyrolysis at 900 °C for 7 min. The pyrolyzed char was naturally cooled to ambient temperature under a nitrogen atmosphere.

Sequential extraction experiments were conducted to determine the different forms of potassium (water-soluble, exchangeable, acid-soluble, and insoluble) in rice husk. The sequential extraction experiment was performed as follows. Rice husk samples were extracted by deionized water at 60 ℃ for 24 h. Then, the rice husk residue was sequentially extracted by ammonium acetate (1.0 $mol{\cdot}L^{-1}$ CH_3COONH_4) and hydrochloric acid (1.0 $mol{\cdot}L^{-1}$ HCl) for 24 h at 60 °C. After acid extraction, the rice husk residue was dissolved in hydrofluoric acid. The ratio of rice husk to extraction solution was always 1: 50 (g/ml). The filtrate was quantitatively analyzed by coupled plasma-optical emission spectroscopy (ICP-OES). Our earlier work [30,31] provides detailed information. Table 2 shows the concentration of different forms of potassium in rice husk.

2.2. Tubular burner system

The tubular burner was comprised of four tangential injectors, each of which was rectangular and 1.5 mm wide, and 6.3 mm high (internally). A high injection velocity promoted rapid mixing. The tubular cyclone flame was contained by a quartz tube with a length of 50 mm and a diameter of 19 mm. Fig. 1 illustrates the schematic of the tubular burner. The Damköhler number (*Da*) (the ratio between the characteristic reaction time and the characteristic mixing time) was less than one in this configuration, indicating the presence of a thoroughly mixed-flow field within the burner, which can thoroughly mix the fuel and oxidizer before the reaction [29,32,33]. The process for calculating the Damköhler number is described in detail in the supplemental materials. Tubular flames were virtually adiabatic and kinetically stable [29], and their gas temperature distribution inside the flame was very uniform after combustion [34,35], making them an excellent heating technique. The turbulence intensity, defined as the ratio of the root mean square of the turbulent velocity fluctuations to the mean velocity, of this tubular burner was between 15% and 179%, while the turbulent intensity of a typical flat flame burner is only 8% [33]. The turbulence intensity distribution in the tubular burner was investigated by CFD and is shown in the supplemental material.

The two tangential injectors that were not contiguous injected a mixture of methane and nitrogen, while the other two injected air-carrying biomass powder. Using a spiral vibrating micro-feeder, the pulverized biomass was fed at a steady rate of 0.7 g/min and a powder feeding concentration of 0.038 Kg/Nm^3. The biomass particle's injection velocity was determined using Dantec's 2D DC PIV (particle image velocimetry) system. There was some uncertainty due to the complex

Table 1
Rice husk's proximate and ultimate analyses.

Sample	Proximate analysis w_{ad}/%				Ultimate analysis w_{ad}/%				
Rice husk	M	A	V	FC	C	H	O	N	S
	7.71	10.23	68.93	12.96	37.14	5.18	39.41	0.30	0.03

Table 2
Analysis of potassium in the rice husk and rice husk char.

Sample	Water-soluble potassium	Exchangeable potassium	Acid-soluble potassium	Insoluble potassium	Total potassium
Rice husk	0.159 (wt %, ad)	0.032 (wt%, ad)	0.005 (wt %, ad)	0.002 (wt %, ad)	0.198 (wt %, ad)
Rice husk char	/	/	/	/	0.152 (wt %, ad)

Note: ad = air-dry basis. The AD (air-dry) basis neglects the presence of moisture other than inherent moisture.

particle size distribution. The measured injection velocity of the biomass particles was 2.53 ± 0.77 m/s, and the standard deviations and measurement results were calculated from four replicate measurements. Referring to an earlier investigation on the single-variable-control method for the Hencken burner system [36–38], this work examined the effect of the ambient CO_2 concentration on the potassium release process and rice husk identification features at a typical temperature of 1150 K. Gas flow rate in different ambiances was shown in Table 3.

A 200 μm type B thermocouple was used to monitor the temperature distribution and compensate for radiation loss. Fig. 2 illustrates the measurement results.

2.3. TDLAS system

Tunable diode laser direct absorption spectroscopy, a line-of-sight technique, has been extensively employed for online flame detection because it does not require complicated signal processing hardware or concentration calibration [24,39,40]. The highest absorption coefficient of K was observed in the D2 ($4^2S_{1/2} \rightarrow 4^2P_{3/2}$) line, which was too close to the oxygen absorption line, so the K(g) D1 ($4^2S_{1/2} \rightarrow 4^2P_{1/2}$) line was chosen. The highest line strength of the K(g) D1 line was 7.43 × 10^6 cm^{-1}/atm (296 K), enabling a K(g) detection limit in the pptv range [41]. The intensity of the D1 line of potassium showed a weak dependence on temperature, varying about 40% from 100 K to 1800 K [41,42].

A schematic diagram of the TDLAS online detection system is shown in Fig. 3. The current-control module and temperature-control module were used to drive a tunable single-mode semiconductor laser (Nanoplus NP-DFB-770-TO56) with a center wavelength of 769.9 nm to scan between 766.94 nm and 770.46 nm with a 30 Hz sawtooth waveform. A photodetector (DTE100A/M, Thorlabs) was used to record changes in the light intensity, and the signal from the photodetector was recorded with a data collector with a sampling frequency of 10 kHz.

From Lambert's law, it follows that,

$$I(\nu) = I_0(\nu)\exp[-\alpha(\nu)] \quad (1)$$

where ν is the frequency of light. $I_0(\nu)$ and $I(\nu)$ are the light intensity before and after absorption, respectively.

The frequency-dependent spectral absorption coefficient $\alpha(\nu)$, which can be expressed as,

Table 3
Gas flow rates in different ambiances.

Combustion style	Average Gas Temperature T (℃) [a]	Fuel mixture components (L/min)			
		CH_4	O_2	N_2	CO_2
Air Combustion	~1150	0.9	3.78	23.22	0
Oxy-fuel combustion	~1150	0.9	5.4	0	21.6

a: Measured using a calibrated B-type thermocouple (Omega)

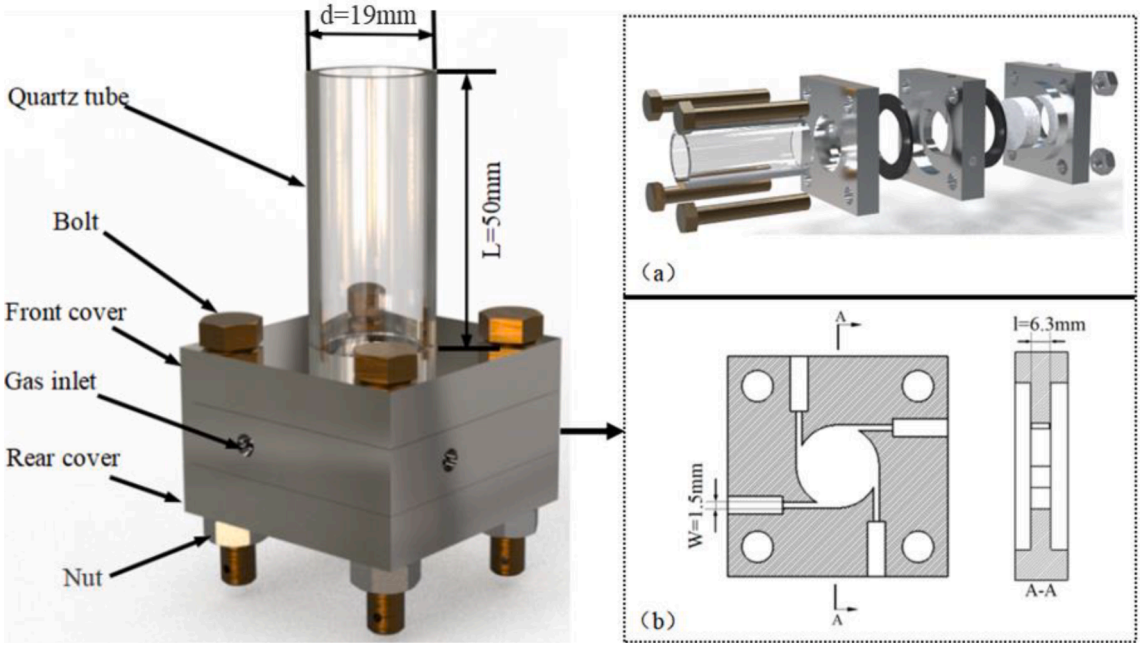

Fig. 1. Schematics of the tubular burner. Details of the injector (a) 3D model of the tubular burner and (b) physical size of the injector.

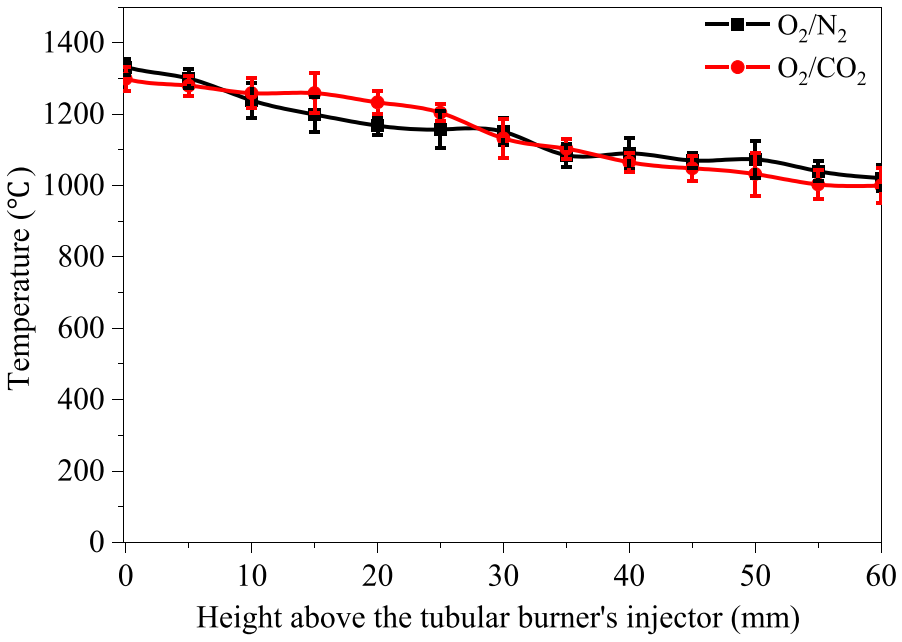

a) Vertical direction at burner's centerline

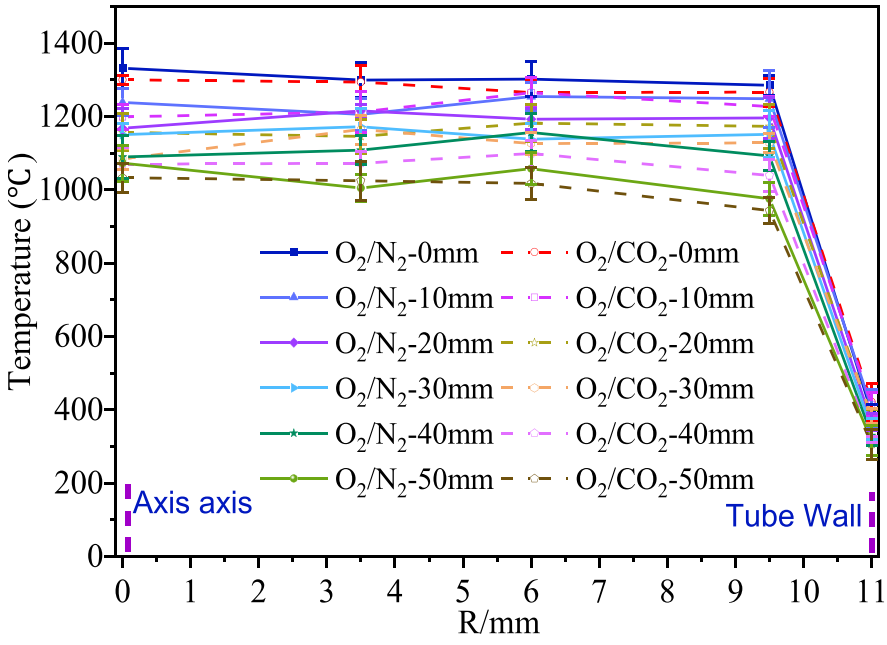

b) Radial direction

Fig. 2. The tubular burner's temperature at N_2/O_2 and CO_2/O_2 atmospheres.

$$\alpha(\nu) = \sigma(\nu)Ln \tag{2}$$

is proportional to the absorption path length L and the molecular number density of the gas (molecule/m^3). $\sigma(\nu)$ is the absorption cross-section (cm^2·$molecule^{-1}$)of the gases, which can be expressed as:

$$\sigma(\nu) = \frac{h\nu_0 B_{12}\varphi(\nu, N, T)}{C} \tag{3}$$

Where, ν_0 is the central frequency, h is Planck's constant, c is the speed of light, φ(v,N,T)is the area-normalized line function, and T is the temperature. B_{12} is the Einstein absorption coefficient, which can be obtained as equation (4) :

$$B_{12} = \left(\frac{g_2}{g_1}\right)\left(\frac{c^3}{8\pi h\nu^3}\right)A_{21} \tag{4}$$

A_{21} is Einstein spontaneous radiation coefficient, For the D1 line of atomic potassium K(g), the degeneracy of states 1 and 2, $g_1 = g_2 = 2$, $A_{21} = 3.75 \times 10^7\ s^{-1}$ [42,43].

First, the absorbance α (ν) is derived from the absorbance equation (1). Voigt profile that describes both doppler spreading and collisional spreading was chosen to perform the absorbing line shape fitting. Equations (2) and (3) then take the integral over the frequencies to derive the number density n can be expressed as.

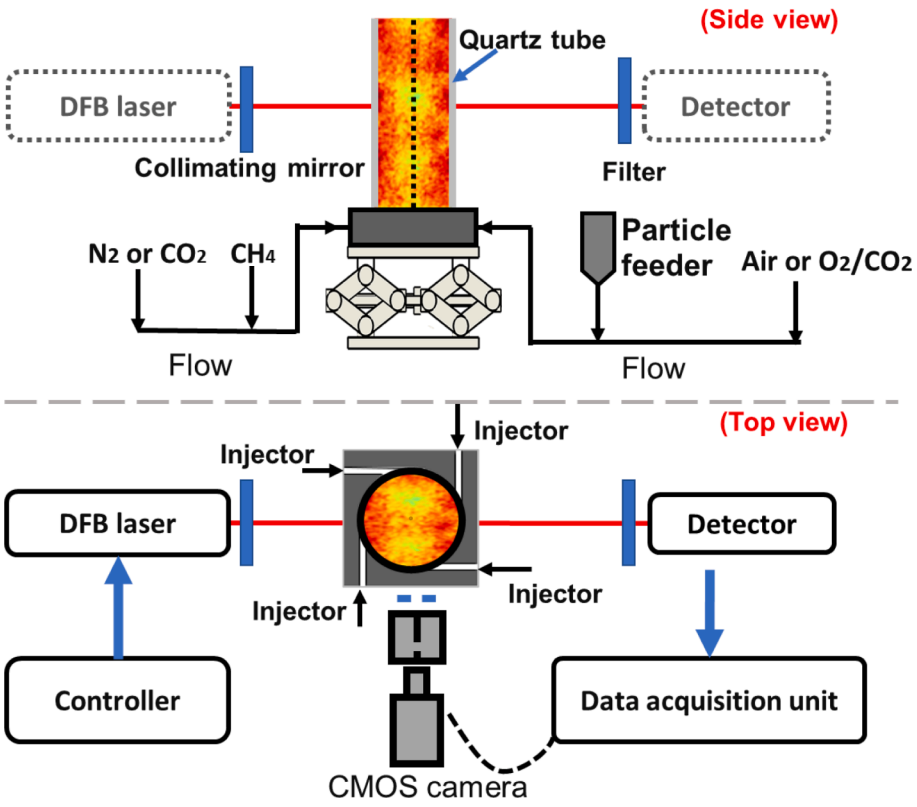

Fig. 3. Schematics for 1D-TDLAS measurement system.

$$n = \frac{c}{h\nu_0 B_{12}^L - \infty} \int \alpha(v) dv \tag{5}$$

$$C = \frac{nM_r}{N_A} \tag{6}$$

C is the concentration, M_r is the relative molecular mass, L is the optical path, and N_A is the Avogadro constant

Since the tubular flame was confined by the quartz tube (inner diameter 1.9 cm), the absorption length is judged by the diameter of the tubular flame. The thickness of the lower temperature region at the edge of the tube wall on both sides was subtracted from the diameter length, and the absorption light path was taken to be 1.5 cm.

Fig. 4 shows the spectra of the D1 line of atomic potassium K(g) obtained from the experiment. Fig. 5 illustrates the measured absorbance spectra (scattered points) of the K(g) D1 line together with the Voigt curve fits (solid lines). According to equation (6), the concentration of K(g)could be deduced. When the concentration was high, the goodness of fit for the absorption line exceeded 0.99. When the K(g) content was as low as 7.35 ppbv, baseline fitting introduced a significant inaccuracy, thus lowering the goodness of fit for the absorption line to 0.7. The lower detection limit for K(g) at 1.5 cm path length was 7 ppbv. The upper detection limit at 1.5 cm path length for K(g) is 1050 ppbv.

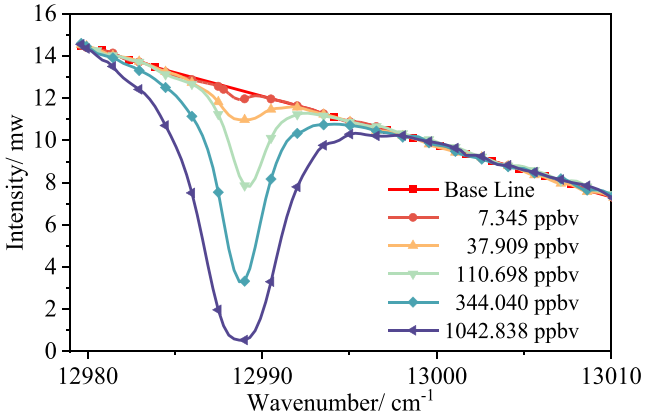

Fig. 4. Scanning spectra of the atomic potassium D1 line.

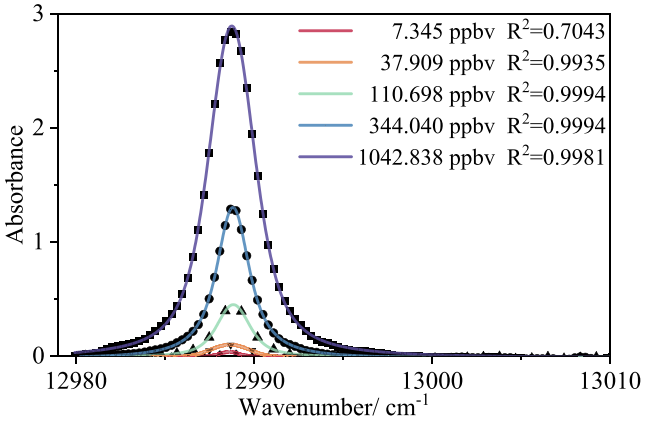

Fig. 5. Measured absorbance spectra (scattered points) of the atomic potassium D1 line together with Voigt curve fits (solid lines) of optical path lengths 1.5 cm.

2.4. Complementary measurement

A digital single-lens mirrorless camera (Sony A7c) was used to take images of pulverized biomass's combustion with an exposure time of 1/24 s, a lens focal length range of 24–70 mm, and a maximum photo size of 5472 × 3648 pixel. These images were then used to investigate the

pulverized biomass's ignition characters.

3. Analysis and discussion

3.1. Ignition and ignition delay detection

Fig. 6 illustrates the dispersed biomass stream's combustion process in a turbulent air combustion environment. As shown in Fig. 6 (a), biomass was rapidly heated by the exhaust gas produced by methane-air combustion and quickly ignited. The purple flame suggests considerable spontaneous potassium radiation in the flame. Some bright upward yellow spirals were also observed, representing the trajectory of the char particles after the devolatilization of biomass. The volatiles spread quickly throughout the combustion chamber due to the cyclonic effect; therefore, there was no visible envelope flame or trailing flame formed around the particles, as when particles are burned on a flat flame burner [1,3]. Compared with rice husk and rice husk char combustion, the color of the flame produced by rice husk char was lighter, and the trajectory of rice husk char particles was brighter. This indicates less spontaneous radiation was produced by the volatiles during rice husk char combustion.

Fig. 7 depicts the solid-phase combustion process of dispersed biomass and char particles after removing the backdrop. The rice husk char solid-phase ignited farther from the burner injector than rice husk, i.e., solid-phase ignition of rice husk particles occurred earlier than char, suggesting that the char particles were more difficult to ignite than biomass particles.

To further clarify the ignition behavior for dispersed biomass in the tubular burner, high-speed images of individual biomass particles combustion were taken, as shown in Fig. 8. To capture the combustion image of individual particles, we dropped the powder feed rate to the lowest possible level, enabling particles to enter the combustion chamber one by one. When biomass was introduced into the burner, it rapidly devolatilized, and the volatile components separated quickly from the char particles due to turbulent flow. Unlike the typical homogeneous ignition mechanism (i.e., sequential combustion of volatiles and char,

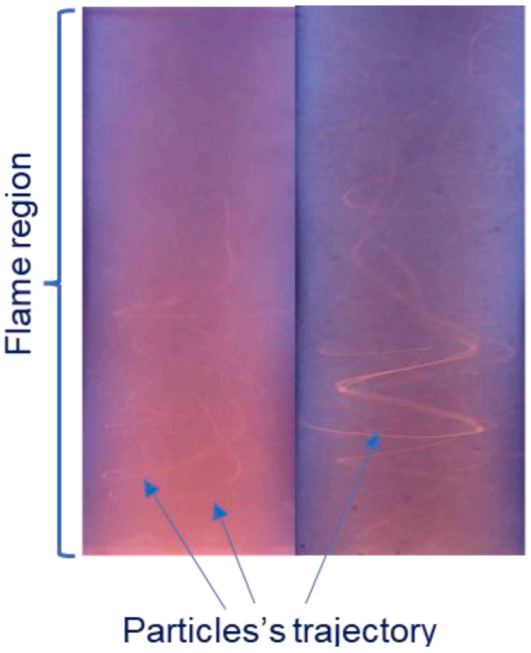

a) Rice husk particles and b) rice husk char particles

Fig. 6. The dispersed biomass stream combustion images on the tubular burner captured by a CMOS camera.

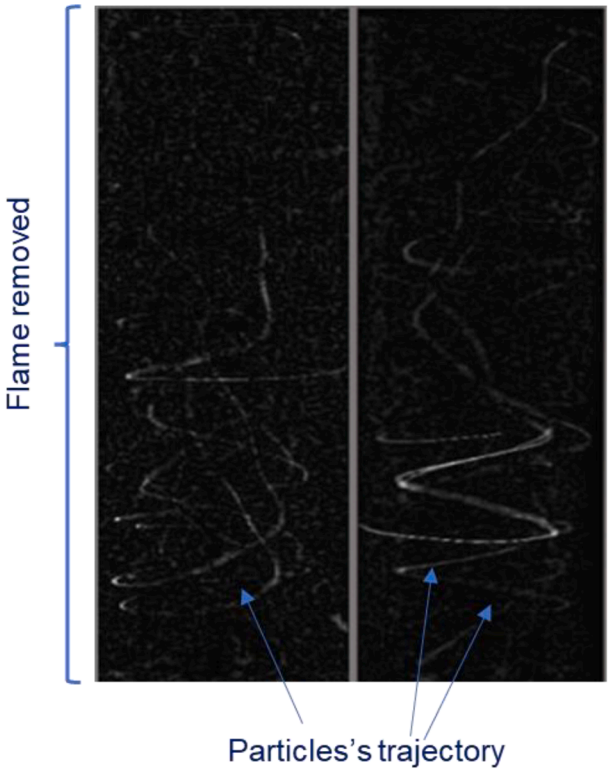

a) Rice husk particles and b) rice husk char particles

Fig. 7. Particles' combustion images of dispersed biomass and char particles.

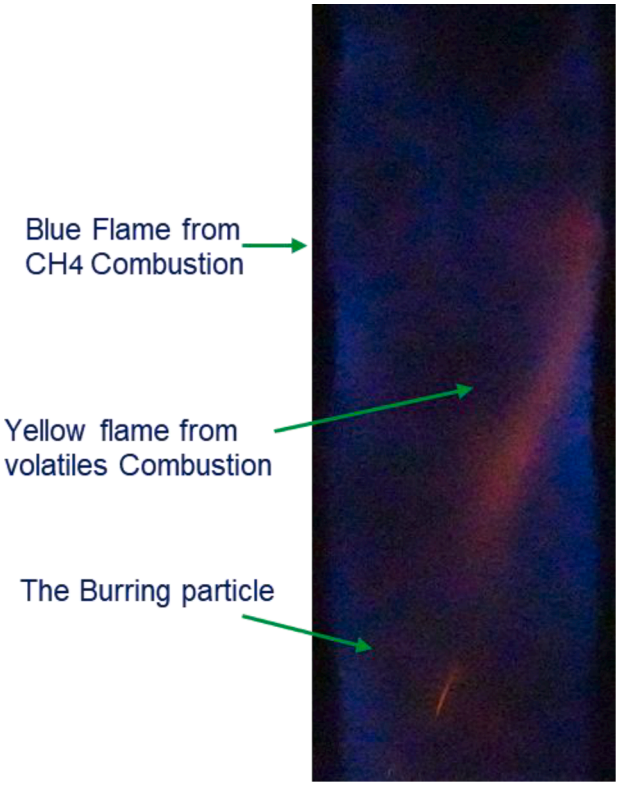

Fig. 8. High-speed imaging of the combustion of individual rice husk particles.

where volatiles ignites first, and then the surface of the pellet ignites at the char surface after the volatiles has burned off) of pulverized biomass on a flat flame or entrained flow reactors with similar atmospheres and temperatures [44], the volatiles combustion and surface combustion of biomass particles could exist simultaneously in a high-temperature, high-turbulence environment, as shown in Fig. 8. There was a clear spatial separation between the volatile fraction and particle surface. We can also see that the solid-phase combustion of biomass occurred slightly away from the burner outlet, lagging behind the volatile fraction combustion in Figs. 6 and 7. Considering the information in Fig. 7 and Fig. 8, we can infer that some rice husk particles in this tubular burner underwent homo-heterogeneous ignition.

The primary factor affecting biomass particle ignition is the heat and mass transport processes occurring inside the particle boundary layer. Compared with pulverized biomass burned in a flat flame jet burner [4,17], the ignition delay was minimized during the combustion of the pulverized biomass in the tubular burner. High-speed cyclonic flow and turbulence enhanced the transport effect around the pellets, significantly reducing the shielding effect of the volatiles on the pellets' surface and allowing for the rapid separation and diffusion of volatiles from biomass pellets. This indicates that turbulence increased heat transfer between the high-temperature flue gas and the rice husk particles' surface and mass transport at the particle boundary. This may also account for the burner's uniform flame color dispersion, as shown in Fig. 6.

3.2. Release characteristics of different forms of potassium

In addition to the baseline fitting error and the Voigt linear function fitting error mentioned in section 2.3, there was also an error due to unavoidable pulsation in the powder feed rate of the spiral vibrating micro-feeder. Fig. 9 shows the real-time TDLAS signal of K(g). Due to irregular fluctuations in the feeding rate over time, the atomic potassium signal showed a non-normal distribution. To eliminate these fluctuations due to powder feed rate pulsations, the median value from 8 s of continuously-collected data was used for each measurement point instead of the average value. The powder feed rate for different fuels was also normalized to 0.7 g/min. (The char feed rate was converted to an air-dry basis)

The concentration of K (g) along the height direction of the burner during rice husk's O_2/N_2 combustion is shown in Fig. 10. As the rice husk entered the burner, the rice husk particles were ignited, with the simultaneous release of K(g). The concentration of K(g) at the burner's injectors reached 0.429 ppm, which gradually decreased with the height above the burner's injectors. This is consistent with the progressive fading of the pink-purple hue of the tubular flame from the bottom to top (the spontaneous emission color of potassium), as shown in the biomass combustion images in Fig. 6. Qu et al. [41] monitored the biomass combustion process online in a carried-flow reactor and also found that K(g) decreased with the increasing distance from the injector. The reduction in the K(g) content along the height above the tubular burner's injectors (from 0 to 50 mm above the injectors) may be attributed to the dilution of methane/air flue gas and transformation of K(g) into other potassium compounds (KOH, KCl, K_2SO_4) [41,45]. Since the flame was confined by the quartz tube, the dilution effect of the surrounding gas on the alkali metal concentration in the flame inside the tube may have only occurred > 50 mm above the burner injector. The initial K(g) concentration may be utilized to evaluate the rate of potassium release.

Comparing the K(g) concentration distribution in the tubular burner during the combustion of rice husk and the other three sequentially-extracted rice husk samples shows that the K(g) concentration decreased gradually after sequential extraction. During the burning of water-washed rice husk, the initial K(g) concentration was just 0.211 ppm. The slower but smoother organic potassium release rate corresponded to the secondary reaction rate of potassium with ash. When comparing the decay rate of the K(g) concentration in the initial stage (burner height 0–5 mm) of rice husk combustion with the combustion of the other three sequentially-extracted rice husk samples, it is apparent that the release of water-soluble potassium mainly occurred in the initial stage of combustion and was the fastest. The release of organic potassium was the slowest process, followed by exchangeable potassium release.

Fig. 11 depicts the concentration distribution of K(g) in a tubular burner during the combustion of rice husk and the other three sequential extracted rice husk under an O_2/CO_2 atmosphere. Unlike in air combustion, the K(g) content decreased more slowly with the height of the tubular burner during rice husk O_2/CO_2 combustion, and the maximum peak value was just 0.263 ppm appearing at 0 mm above the burner's injector, which was considerably lower than that during air combustion. Compared with the air environment, the potassium release process shifted from a quick and intense model to a continuous and slow-release one during rice husk burning. The K(g) concentration distribution in the tubular burner was the same for water-washed rice husk, NH_3Ac-washed rice husk, and acid-washed rice husk during air combustion and O_2/CO_2 combustion, which gradually decreased along with increasing the burner height. When the four fuels were combusted in O_2/CO_2 and O_2/N_2 atmospheres, the O_2/CO_2 atmosphere had little effect on the distribution of the K(g) concentration during the combustion of water-washed rice husk, acid-washed rice husk, and NH_3Ac-washed rice husk in the tubular burner; however, it had a more significant inhibitory effect during rice husk combustion. This indicates that the O_2/CO_2 atmosphere had a more significant impact on water-soluble potassium and only a slight impact on the release of exchangeable and organic potassium.

3.3. Potassium release characteristics during bio-char combustion

Fig. 12 illustrates the distribution of K(g) concentration during rice husk and rice husk char air combustion in the tubular burner. During rice husk char combustion, there was a lower K(g) concentration at 0–35 mm above the tubular burner's injectors compared with rice husk

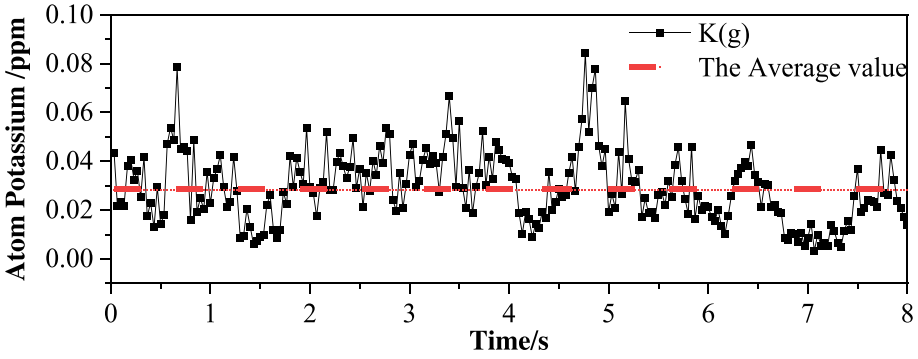

Fig. 9. Real-time TDLAS data for K(g) concentration.

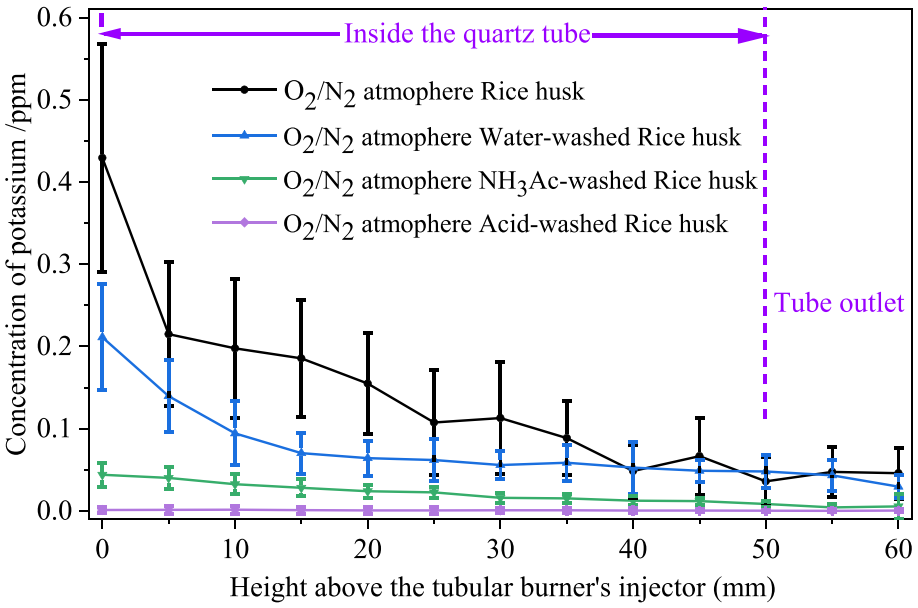

Fig. 10. The concentration of K (g) along the height direction of the burner during rice husk's O_2/N_2 combustion. Error bars represent the standard deviation caused by the biomass feed system fluctuations.

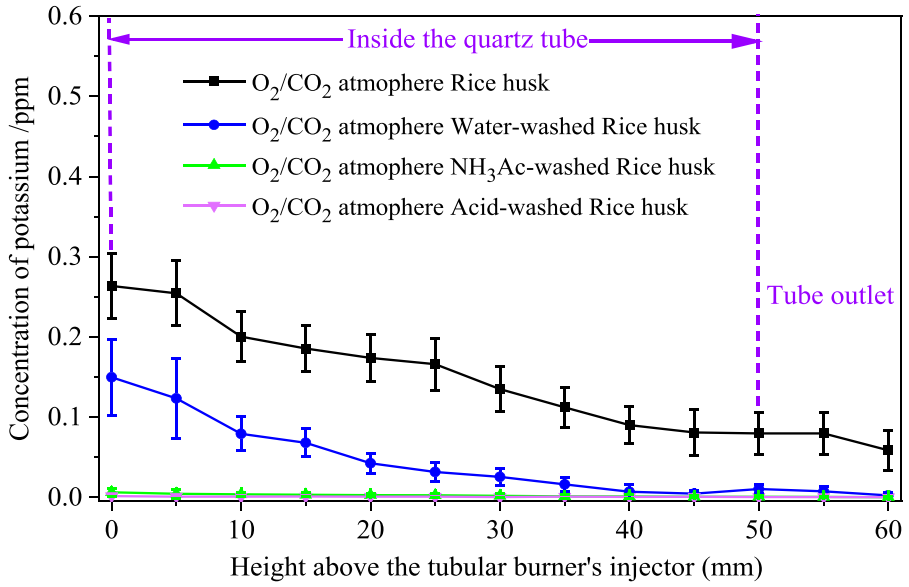

Fig. 11. The K (g) concentration along the burner's height direction during four fuels' O_2/CO_2 combustion (Rice husk, water-washed rice husk, NH_3Ac-washed rice husk, and acid-washed rice husk). Error bars represent the standard deviation caused by the biomass feed system fluctuations.

combustion. The difference between the release process of K(g) during the combustion of rice husk and rice husk char was mainly due to the fact that some potassium was released during the char production process, and no volatiles was produced during the combustion of rice husk char. When rice husk char was burned, the K(g) concentration at 0 mm was only slightly higher than that at 5 mm, indicating that the release process of potassium enriched in char took a long time but had a low release rate. The K(g) concentration 0 mm above the burner's injector during rice husk combustion was nearly twice as high as during rice husk char combustion. Similarly, 40–60% of potassium in biomass is released during the volatile fraction combustion stage during biomass single-pellet combustion observed in previous investigations [19,21].

The K(g) concentration distribution during rice husk and rice husk char combustion under an O_2/CO_2 atmosphere in the tubular burner is shown in Fig. 13. When rice husk was combusted under an O_2/CO_2 atmosphere, the K(g) concentration was suppressed and displayed a slow decline with the height of the burner, in contrast to the O_2/N_2 atmosphere. This also indicates that the potassium release process in the O_2/CO_2 atmosphere was longer but slower. During rice husk char combusted in an O_2/CO_2 atmosphere, the decline in the K(g) concentration along the height direction of the burner was relatively similar to that in an O_2/N_2 atmosphere.

Previous studies have suggested that the presence of CO_2 reduces the ignition of volatiles in envelope flames under active gas flow [46]. The additional gaseous flame radiation from CO_2 and the higher specific heat capacity increased the ignition delay [47]. The char surface's temperature under an O_2/CO_2 atmosphere was lower than that of the char's surface under an O_2/N_2 atmosphere caused by the lower diffusivity of O_2

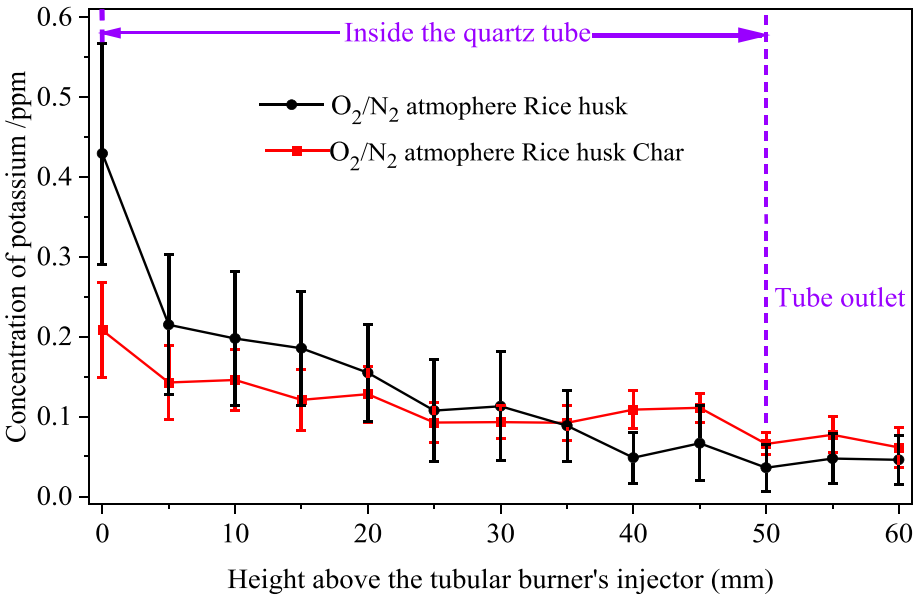

Fig. 12. The concentration of K (g) along the height direction of the burner during rice husk/char's O_2/N_2 combustion. Error bars represent the standard deviation caused by the biomass feed system fluctuations.

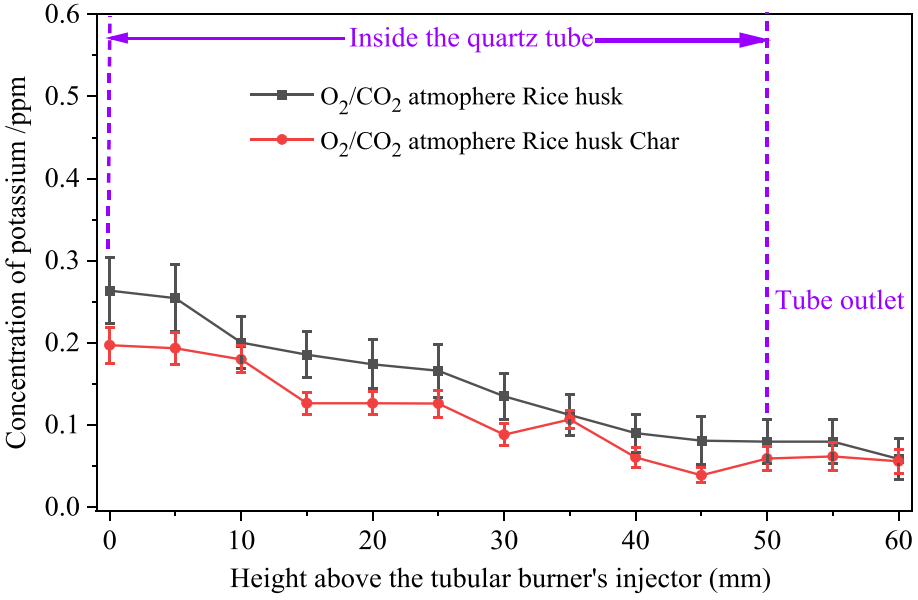

Fig. 13. The concentration of K (g) along the height direction of the burner during rice husk/rice husk char's O_2/ CO_2 combustion. Error bars represent the standard deviation caused by the biomass feed system fluctuations.

in CO_2 than in N_2 [48]. This may be one explanation for the low rate of potassium release during rice husk char combustion in an O_2/CO_2 atmosphere.

The K(g) concentration at 0 mm from the burner injector was 0.42 ppm during air combustion, while that decreased by 35.72 % of O_2/CO_2 combustion with a 0.27 ppm. The initial concentrations of atomized potassium in the air combustion and O_2/CO_2 combustion processes of rice husk char were 0.208 ppm and 0.197 ppm, respectively. O_2/CO_2 combustion resulted in a 5.29% reduction in K(g) concentration here during rice husk char combustion. We can see that the inhibitory effect of the O_2/CO_2 atmosphere on the potassium release during rice husk char combustion was relatively weak compared with rice husk combustion. As previously mentioned, the rice husk combustion process was homo-heterogeneous ignition in the tubular burner. Both combustions of volatiles and char could be inhibited during rice husk's O_2/CO_2 atmosphere. There was no volatiles combustion during char combustion, making the O_2/CO_2 atmosphere have a weaker suppressions effect. Therefore, we might speculate that the O2/CO2 atmosphere suppresses the release of potassium primarily via the suppression of volatile combustion and, to a lesser degree, by inhibiting char combustion. As section 3.2 observed, the O_2/CO_2 atmosphere also has a more significant impact on the water-soluble state of potassium and the inhibitory effect of the O_2/CO_2 atmosphere on the potassium release during rice husk was more pronounced compared with rice husk char combustion. Since we may speculate that the water-soluble form of potassium is mainly associated with the volatile's combustion process rather than char combustion.

4. Discussion

Since the gas flow rate and biomass fuel feed rate are fixed in the

experiment, this experiment is a steady combustion system when ignoring the error due to unavoidable pulsation in the powder feed rate of the spiral vibrating micro-feeder. The distribution of physical quantities such as temperature and species distribution in the burner does not change with time.

TDLAS technology, similar to LIBS/PLIF, can only determine atomic potassium concentrations but cannot directly obtain the content of all potassium-containing species. To investigate the stable species, present in the gas phase, thermodynamic equilibrium calculations have been widely used to infer the absolute content of total alkali metal elements during coal/biomass pellet combustion in a planar flame [9,13,18]. Thermodynamic equilibrium calculations are based on the assumption that a system's residence time is much longer than the chemical kinetic time scale and that all species are mixed uniformly [49,50]. Our current experimental work found that the dilution or conversion of atomic potassium into other potassium compounds (KOH, KCl, and K_2SO_4) in a highly turbulent environment were far more intense than in a flat flame. It is challenging to accurately determine the region where K(g), KCl(g), and KOH (g) are in equilibrium in the tubular burner.

Due to this challenge, the current work attempted to estimate the release rate of atomic potassium, the proportion of released atomic potassium to total potassium in the particles, at the beginning point (0 mm above injectors) rather than the absolute release rate of total potassium, as detailed in Table 4. Compare with 50 mm above injectors, the biomass's movement from the injector to 0 mm above injectors was very fast. Since this, a model hypothesis was made for the estimation of the proportion of released atomic potassium to initial total potassium in the particles at 0 mm above injectors, i.e., the dilution or migration of the K(g) during biomass's movement from the injector to 0 mm above injectors was neglected. The release ratio of atomic potassium was confined as the Proportion of released K(g) to total initial potassium in the particles.

At 0 mm above the burner injector, the release ratio of K(g), the proportion of released atomic potassium in initial total potassium in particles, was 1.38% for rice husk combustion and 0.8% for O_2/CO_2 combustion of rice husk, slightly higher than the 0.79% release ratio of atomic potassium measured for air combustion of biomass pellets on a flat flame at around 1300 K in a flat flame [19]. This might because the heat and mass transfer efficiency of biomass particles in a high turbulence environment with high temperature flue gas is much higher than that in a flat flame plume, accelerating the release of atomic potassium, or it might be because atomic potassium had not been transformed into potassium compounds such as KOH(g) and KCl(g) in time. Here, in situ measurements of more extensive potassium compounds are required for further investigation.

The K(g) flux during the combustion of rice husk is higher than the water-washed and NH_3Ac-washed rice husk. While the release ratio of K (g), the proportion of released K(g) in initial total potassium in particles from water-washed and NH_3Ac-washed rice husk are higher than that from rice husk combustion. This may be due to the fact that after water washing and NH_3Ac washing, only organically bound potassium (potassium coordinated with carboxyl oxygen, hydroxyl itch, or carbonyl oxygen) [51] remains in the biomass, and the organic potassium in the biomass may be released as K(g). Inorganic potassium may be released mainly as KOH(g), KCl(g), and a small proportion with K(g). 80% of the potassium in the rice husk is inorganic potassium, which is mainly released in the form of KOH(g) and KCl(g) [50,52], thus making the released atomic potassium a smaller proportion of the total potassium in the original rice husk particles.

The release ratio of atomic potassium from rice husk combustion is lower than that from rice husk, under O_2/CO_2 and air combustion conditions. This may be due to the relatively high ash ratio in the char and the adsorption of potassium atoms by the silica-aluminates in the ash during combustion.

To a deeper understanding of the potassium release and its migration transformation processes, in the future works will combine TDLAS, UV broadband absorption to monitor both K(g), KOH(g), simultaneously. On the other hand, CFD with the detailed reaction mechanism of alkali metals and the condensation process of the particulate matter is also significant.

5. Conclusions

In this work, the release process of potassium from rice husk in a tubular burner for the first time was monitored online using visible light detection and calibration-free TDLAS techniques. The effect of different treatments of pulverized biomass on potassium release and pulverized rice husk's ignition characteristics in a turbulent environment were discussed, and the following main conclusions were obtained.

High-speed cyclonic flow and turbulence enhanced the transport effect around the particles, significantly reducing the shielding effect of the volatiles on the particles' surface and allowing for the rapid separation and diffusion of volatiles from biomass particles. The ignition delay in the tubular burner was significantly shorter than that of pulverized biomass when the same particle size was burned on a flat-flame burner. Meanwhile, high-speed photography validated the occurrence of homo-heterogeneous ignition.

The slower but smoother release rate of organic potassium in the exchangeable or acid-soluble state indicates that the release rate of organic potassium was comparable to the secondary reaction rate of potassium with ash. The release of water-soluble potassium is the fastest. The release of organic potassium is the slowest, followed by exchangeable potassium. The release ratio of atomic potassium from water-washed and NH_3Ac-washed rice husk is higher than that from rice husk combustion under O_2/CO_2 and air combustion conditions. The release of potassium enriched in char took a long time but had a low release rate. Comparing the distribution of potassium in the burner when the four fuels were combusted in O_2/CO_2, and O_2/N_2 atmospheres, the O_2/CO_2 atmosphere had little effect on the K(g) concentration distribution during the combustion of water-washed rice husk, acid-washed rice husk, and NH_3Ac-washed rice husk in the tubular burner, but it had a more significant inhibitory effect during the combustion of rice husk. The inhibitory effect of the O_2/CO_2 atmosphere on the potassium release during rice husk char combustion was relatively weak compared with

Table 4
Proportion of released K(g) to total initial potassium in the particles at 0 mm above injectors.

	N_2/O_2 combustion					O_2/CO_2 combustion				
	Rice husk	Water-washed Rice husk	NH_3Ac-washed Rice husk	Acid-washed Rice husk	Rice huskchar	Rice husk	Water-washed Rice husk	NH_3Ac-washed Rice husk	Acid-washed Rice husk	Rice husk char
Atomic potassium K(g) Proportion (wt%) [a]	1.38	3.49	4.06	0.37	0.88	0.80	2.31	0.53	0.43	0.78
Atomic potassium K(g) Proportion (wt%) by CHEMKIN [a]	0.68% −1.2% at 1300 K [13,19], vary by initial potassium form									

a: based on initial potassium in the particle

rice husk combustion.

CRediT authorship contribution statement

Sun Cen: Conceptualization, Methodology, Software, Investigation, Data curation, Validation, Visualization, Writing – review & editing. **Wei Xiaolin:** Funding acquisition, Writing – review & editing. **Li Teng:** Methodology. **Zhou Li:** Methodology, Investigation. **Teng Qinzheng:** Investigation. **Li Sen:** Methodology, Writing – review & editing.

Declaration of Competing Interest

The authors declare that they have no known competing financial interests or personal relationships that could have appeared to influence the work reported in this paper.

Acknowledgment

The Key Project of the National Natural Science Foundation of China supported this work (No. 51736010). Cen Sun, thanks for the discussion with Professor Fei Li, Professor Baolu Shi, Professor Chunbo Wang, Dr. Aixue Zhu, Dr. Huixin Li, Dr. Running Kang, and Dr. Jing Zhao.

Appendix A. Supplementary data

Supplementary data to this article can be found online at https://doi.org/10.1016/j.fuel.2022.123570.

References

[1] Simões G, et al. effect of gas temperature and oxygen concentration on single particle ignition behavior of biomass fuels. Proc Combust Inst 2017;36(2):2235–42. https://doi.org/10.1016/j.proci.2016.06.102.
[2] Si M, et al. Study on the combustion behavior and soot formation of single coal particle using hyperspectral imaging technique. Combust Flame 2021;233:111568. https://doi.org/10.1016/j.combustflame.2021.111568.
[3] Qi S, et al. Ignition and combustion of single pulverized biomass and coal particles in N_2/O_2 and CO_2/O_2 environments. Fuel 2021;283:118956. https://doi.org/10.1016/j.fuel.2020.118956.
[4] Fatehi H, et al. Numerical simulation of ignition mode and ignition delay time of pulverized biomass particles. Combust Flame 2019;206:400–10. https://doi.org/10.1016/j.combustflame.2019.05.020.
[5] Wen X, et al. Flamelet LES of a swirl-stabilized multi-stream pulverized coal burner in air and oxy-fuel atmospheres with pollutant formation. Proc Combust Inst 2021;38(3):4141–9. https://doi.org/10.1016/j.proci.2020.05.061.
[6] Krüger J, Haugen NEL, Løvås T. Correlation effects between turbulence and the conversion rate of pulverized char particles. Combust Flame 2017;185:160–72. https://doi.org/10.1016/j.combustflame.2017.07.008.
[7] Zhang W, Watanabe H, Kitagawa T. Direct numerical simulation of ignition of a single particle freely moving in a uniform flow. Adv Powder Technol 2017;28(11):2893–902. https://doi.org/10.1016/j.apt.2017.08.016.
[8] Meller D, et al. Numerical Analysis of a Turbulent Pulverized Coal Flame Using a Flamelet/Progress Variable Approach and Modeling Experimental Artifacts. Energy Fuels 2021;35(9):7133–43. https://doi.org/10.1021/acs.energyfuels.0c03477.
[9] van Eyk PJ, et al. The release of water-bound and organic sodium from Loy Yang coal during the combustion of single particles in a flat flame. Combust Flame 2011;158(6):1181–92. https://doi.org/10.1016/j.combustflame.2010.10.024.
[10] VanEyk PJ, et al. Quantitative measurement of atomic sodium in the plume of a single burning coal particle. Combust Flame 2008;155(3):529–37. https://doi.org/10.1016/j.combustflame.2008.05.012.
[11] Wang Z, et al. Measurement of atomic sodium release during pyrolysis and combustion of sodium-enriched Zhundong coal pellet. Combust Flame 2017;176:429–38. https://doi.org/10.1016/j.combustflame.2016.10.020.
[12] Weng W, et al. Quantitative imaging of potassium release from single burning pulverized biomass char particles. Fuel 2020;264:116866. https://doi.org/10.1016/j.fuel.2019.116866.
[13] Fatehi H, et al. Modeling of alkali metal release during biomass pyrolysis. Proc Combust Inst 2017;36(2):2243–51. https://doi.org/10.1016/j.proci.2016.06.079.
[14] Hsu L, et al. Sodium and Potassium Released from Burning Particles of Brown Coal and Pine Wood in a Laminar Premixed Methane Flame Using Quantitative Laser-Induced Breakdown Spectroscopy. Appl Spectrosc 2011;65(6):684–91. https://doi.org/10.1366/10-06108.
[15] He Y, et al. In-situ Measurement of Sodium and Potassium Release during Oxy-Fuel Combustion of Lignite using Laser-Induced Breakdown Spectroscopy: Effects of O_2 and CO_2 Concentration. Energy Fuels 2013;27(2):1123–30. https://doi.org/10.1021/ef301750h.
[16] He Y, et al. Inhibition of Sodium Release from Zhundong Coal via the Addition of Mineral Additives: Online Combustion Measurement with Laser-Induced Breakdown Spectroscopy (LIBS). Energy Fuels 2017;31(2):1082–90. https://doi.org/10.1021/acs.energyfuels.6b01673.
[17] He Y, et al. Release characteristic of different classes of sodium during combustion of Zhun-Dong coal investigated by laser-induced breakdown spectroscopy. Science Bulletin 2015;60(22):1927–34. https://doi.org/10.1007/s11434-015-0922-9.
[18] Liu Y, et al. Multi-point LIBS measurement and kinetics modeling of sodium release from a burning Zhundong coal particle. Combust Flame 2018;189:77–86. https://doi.org/10.1016/j.combustflame.2017.10.026.
[19] Liu Y, et al. Measurement and kinetics of elemental and atomic potassium release from a burning biomass pellet. Proc Combust Inst 2019;37(3):2681–8. https://doi.org/10.1016/j.proci.2018.06.042.
[20] Yuan Y, Li S, Yao Q. Dynamic behavior of sodium release from pulverized coal combustion by phase-selective laser-induced breakdown spectroscopy. Proc Combust Inst 2015;35(2):2339–46. https://doi.org/10.1016/j.proci.2014.07.016.
[21] He Z, et al. Experimental investigation on temporal release of potassium from biomass pellet combustion by flame emission spectroscopy. Fuel 2019;253:1378–84. https://doi.org/10.1016/j.fuel.2019.05.133.
[22] Li K, et al. In-situ measurement of temperature and potassium concentration during the combustion of biomass pellets based on the emission spectrum. Fuel 2021;289:119863. https://doi.org/10.1016/j.fuel.2020.119863.
[23] Sepman A, et al. Real-time in situ multi-parameter TDLAS sensing in the reactor core of an entrained-flow biomass gasifier. Proc Combust Inst 2017;36(3):4541–8. https://doi.org/10.1016/j.proci.2016.07.011.
[24] Monkhouse P. Online diagnostic methods for metal species in industrial process gas. Prog Energy Combust Sci 2002;28(4):331–81. https://doi.org/10.1016/S0360-1285(02)00006-0.
[25] Qu Z, et al. Tunable Diode Laser Atomic Absorption Spectroscopy for Detection of Potassium under Optically Thick Conditions. Anal Chem 2016;88(7):3754–60. https://doi.org/10.1021/acs.analchem.5b04610.
[26] Weng W, et al. Quantitative Measurement of Atomic Potassium in Plumes over Burning Solid Fuels Using Infrared-Diode Laser Spectroscopy. Energy Fuels 2017;31(3):2831–7. https://doi.org/10.1021/acs.energyfuels.6b02638.
[27] Mock C, et al. Combustion Behavior of Relatively Large Pulverized Biomass Particles at Rapid Heating Rates. Energy Fuels 2016;30(12):10809–22. https://doi.org/10.1021/acs.energyfuels.6b01457.
[28] Panahi A, et al. On the particle sizing of torrefied biomass for co-firing with pulverized coal. Combust Flame 2018;194:72–84. https://doi.org/10.1016/j.combustflame.2018.04.014.
[29] Wei J, et al. Effects of temperature-time history on the flame synthesis of nanoparticles in a swirl-stabilized tubular burner with two feeding modes. J Aerosol Sci 2019;133:72–82. https://doi.org/10.1016/j.jaerosci.2019.04.002.
[30] Li Huijun, et al., Experimental study on occurrence of alkali metals in rice husk. Electric Power Science and Engineering, 2019. 35(06): p. 58-63. CNKI:SUN:DLQB.0.2019-06-009.
[31] Li Huijun, et al., Release characteristics of alkali metals during wheat straw burning. Clean Coal Technology, 2019. 25(02): p. 62-68. CNKI: SUN: JJMS.0.2019-02-008.
[32] Hu J , Shi B , Shimokuri D , et al. An experimental study on the heating process with a tubular flame. 2013.
[33] Xu Y, et al. investigation on ignition behaviors of pulverized coal particles in a tubular swirl burner. Proc Combust Inst 2021;38(3):4179–88. https://doi.org/10.1016/j.proci.2020.07.131.
[34] Hirano T, et al. Tubular Flame Combustion for Nanoparticle Production. Ind Eng Chem Res 2019;58(17):7193–9. https://doi.org/10.1021/acs.iecr.9b00620.
[35] Zhao X, et al. Effects of N_2 and CO_2 dilution on the combustion characteristics of C_3H_8/O_2 mixture in a swirl tubular flame burner. Exp Therm Fluid Sci 2019;100:251–8. https://doi.org/10.1016/j.expthermflusci.2018.09.009.
[36] Shan S, et al. Spectral radiation characteristics in semi-coke jet flame for energy utilization. Fuel 2021;302:121194. https://doi.org/10.1016/j.fuel.2021.121194.
[37] Yuan Y, et al. Experimental and theoretical analyses on ignition and surface temperature of dispersed coal particles in O_2/N_2 and O_2/CO_2 ambients. Fuel 2017;201:93–8. https://doi.org/10.1016/j.fuel.2016.09.079.
[38] Xu Y, et al. investigation of steam effect on ignition of dispersed coal particles in O_2/N_2 and O_2/CO_2 ambiences. Fuel 2018;233:388–95. https://doi.org/10.1016/j.fuel.2018.06.047.
[39] Schlosser E, et al. In situ detection of potassium atoms in high-temperature coal-combustion systems using near-infrared-diode lasers. Spectrochim Acta A Mol Biomol Spectrosc 2002;58(11):2347–59. https://doi.org/10.1016/S1386-1425(02)00049-5.
[40] Zhao W, et al. A WMS Based TDLAS Tomographic System for Distribution Retrievals of Both Gas Concentration and Temperature in Dynamic Flames. IEEE Sens J 2020;20(8):4179–88. https://doi.org/10.1109/JSEN.2019.2962736.
[41] Qu Z, et al. Distribution of temperature, H_2O and atomic potassium during entrained flow biomass combustion–Coupling in situ TDLAS with modeling approaches and ash chemistry. Combust Flame 2018;188:488–97. https://doi.org/10.1016/j.combustflame.2017.10.013.
[42] Ding Y, et al. Shock tube measurements of high-temperature argon broadening and shift parameters for the potassium D1 and D2 resonance transitions. J Quant Spectrosc Radiat Transfer 2021;275:107895. https://doi.org/10.1016/j.jqsrt.2021.107895.
[43] Sansonetti JE, Martin WC. Handbook of Basic Atomic Spectroscopic Data. J Phys Chem Ref Data 2005;34(4):1559–2259. https://doi.org/10.1063/1.1800011.

[44] Magalhães D, et al. Ignition behavior of Turkish biomass and lignite fuels at low and high heating rates. Fuel 2017;207:154–64. https://doi.org/10.1016/j.fuel.2017.06.069.
[45] Boström D, et al. Ash Transformation Chemistry during Combustion of Biomass. Energy Fuels 2011;26(1):85–93. https://doi.org/10.1021/ef201205b.
[46] Khatami R, Stivers C, Levendis YA. Ignition characteristics of single coal particles from three different ranks in O_2/N_2 and O_2/CO_2 atmospheres. Combust Flame 2012;159(12):3554–68. https://doi.org/10.1016/j.combustflame.2012.06.019.
[47] Liu D, et al. Transformation characteristics of sodium, chlorine and sulfur of Zhundong coal during O_2/CO_2 combustion in circulating fluidized bed. Energy 2019;185:254–61. https://doi.org/10.1016/j.energy.2019.07.043.
[48] Lei M, Sun C, Zhang Y. Investigation on the physicochemical properties of coal char during pressurized pyrolysis and the mineral transformations of coal ash during pressurized O_2/ N_2 and O_2/CO_2combustion. Int J Energy Res 2020. https://doi.org/10.1002/er.5739.
[49] Glarborg P, Marshall P. Mechanism and modeling of the formation of gaseous alkali sulfates. Combust Flame 2005;141(1–2):22–39. https://doi.org/10.1016/j.combustflame.2004.08.014.
[50] van Eyk PJ, Ashman PJ, Nathan GJ. Mechanism and kinetics of sodium release from brown coal char particles during combustion. Combust Flame 2011;158(12):2512–23. https://doi.org/10.1016/j.combustflame.2011.05.005.
[51] Sun C, et al. Intrinsic sodium occurrence in Zhundong coal: Experimental observations and molecular modeling. Fuel 2021;305:121491. https://doi.org/10.1016/j.fuel.2021.121491.
[52] Li X, Li C. Volatilisation and catalytic effects of alkali and alkaline earth metallic species during the pyrolysis and gasification of Victorian brown coal. Part VIII. Catalysis and changes in char structure during gasification in steam. Fuel 2006;85(10–11):1518–25. https://doi.org/10.1016/j.fuel.2006.01.007.